Backward nucleon production by heavy baryonic resonances in proton-nucleus collisions

Oleksandra Panova,[1,*] Anton Motornenko,[2,3] Mark I. Gorenstein,[4,3] Jan Steinheimer,[3] and Horst Stoecker[2,3,5]

[1]*Taras Shevchenko National University of Kyiv, Kyiv, Ukraine*
[2]*Institut für Theoretische Physik, Goethe Universität, D-60438 Frankfurt am Main, Germany*
[3]*Frankfurt Institute for Advanced Studies, Giersch Science Center, D-60438, Frankfurt am Main, Germany*
[4]*Bogolyubov Institute for Theoretical Physics, Kyiv, Ukraine*
[5]*GSI Helmholtzzentrum für Schwerionenforschung GmbH, D-64291 Darmstadt, Germany*

(Received 15 August 2019; published 20 November 2019)

The production of backward nucleons, $N(180^\circ)$, at 180° in the nuclear target rest frame in proton-nucleus $(p+A)$ collisions is studied. The backward nucleons appearing outside of the kinematically allowed range of proton-nucleon $(p+N)$ reactions are shown to be due to secondary reactions of heavy baryonic resonances produced inside the nucleus. Baryonic resonances R created in primary $p+N$ reactions can change their masses and momenta due to successive collisions $R+N \to R+N$ with other nuclear nucleons. Two distinct mechanisms and kinematic restrictions are studied: the reaction $R+N \to N(180^\circ)+N$ and the resonance decay $R \to N(180^\circ)+\pi$. Simulations of $p+A$ collisions using the Ultrarelativistic Quantum Molecular Dynamics model support these mechanisms and are consistent with available data on proton backward production.

DOI: 10.1103/PhysRevC.100.054617

I. INTRODUCTION

A large fraction of the particles produced in inelastic nucleon-nucleon $(N+N)$ collisions fraction appears from the decays of meson and baryon resonances, e.g., from Δ and N^* isobars, which decay subsequently into a stable baryon and one or more mesons, dileptons, or photons. The large number of resonance states and their large decay widths have led Hagedorn to postulate that the resonance mass spectrum behaves as a continuous exponentially increasing function [1]. This is indeed experimentally found up to masses of approximately 3 GeV [2], larger masses are not easily identified. An exponentially increasing mass spectrum $\rho(m) \sim \exp(m/T_{\rm H})$ of the hadronic states at $m \to \infty$ leads to the limiting temperature $T = T_{\rm H}$ for strongly interacting matter. Later theoretical suggestions [3–5] transformed the concept of a limiting temperature to the concept of a temperature of a phase transition or a crossover to a new high-temperature state—the quark-gluon plasma. The crossover model with Hagedorn states does indeed describe the lattice QCD data [6]. Microscopic transport models of high-energy collisions [7–11] model the Hagedorn states by string excitations [12] or include them directly [13].

Experimentally produced nucleons emitted in proton-nucleus $(p+A)$ collisions have been observed in backward direction, at 180°, in the nuclear target rest frame [these nucleons will be further denoted as $N(180^\circ)$ and named *backward* nucleons). Note that the backward nucleons appear in a kinematic region forbidden in binary proton-proton $(p+p)$ reactions. The production of backward nucleons and mesons was observed experimentally [14,15] and is referred to as a "cumulative effect" since two or more nuclear nucleons should be involved in this process. Several models were proposed to explain the data. One group of models suggests that an extension of the kinematic limit of nucleon-nucleon $(N+N)$ collision is possible in $p+A$ reactions due to the short-range proton-neutron correlations in the nuclear target [16–21]. These correlations lead to the presence of long tails in the nucleon momentum distributions inside a nucleus and thus extend the kinematic region of the emitted particles in $p+A$ reactions. It was also suggested that the cumulative effect is a result of the presence of multinucleon targets ("grains") with masses $2m$, $3m$, ... (where m is the nucleon mass) inside the nucleus (see Refs. [22–26]). In both these explanations, all necessary requisites for the cumulative hadron production are present inside the nucleus before the $p+A$ reaction.

Our present study is based on an alternative model scenario [27], see also Refs. [28–35]. The kinematically forbidden regions in $N+N$ collisions can be explored in $p+A$ reactions due to creation of heavy hadronic states and their successive collisions with nuclear nucleons. We assume that a heavy baryonic resonance R, created in a primary proton-nucleon $(p+N)$ reaction, can propagate further through the nucleus, and it has a chance to interact with another nuclear nucleon earlier than its decay to a stable hadron occurs. Therefore, several nuclear nucleons are involved in the backward nucleon production. Two mechanisms for the production of a backward nucleon $N(180^\circ)$ will be considered: the reaction $R+N \to N(180^\circ)+N$ and the resonance decay to nucleon and pion $R \to N(180^\circ)+\pi$.

Excitations of heavy baryonic states and their subsequent rescattering can be also probed in the subthreshold production [36–38] of massive hadrons in $A+A$ collisions. Recently this approach was used to describe the data on strange and charm

*Corresponding author: panova.oleksandra@gmail.com

particle production [39–41]. The two phenomena in $p+A$ reactions—the production of hadrons outside the kinematic region of $N+N$ collisions and the subthreshold production of strange and charmed heavy hadrons—have probably the same origin, namely, the creation of heavy resonances and their further interactions with nuclear nucleons.

This paper is organized as follows. In Sec. II we calculate the maximal energy for the backward production of nucleons in $p+A$ reactions if $n=2,3,\ldots$ nuclear nucleons are involved in this reaction. The mass of the baryonic resonance needed for this production is also calculated. These results are obtained as a consequence of energy-momentum conservation. In Sec. III the results of the Ultrarelativistic Quantum Molecular Dynamics simulations are presented. Section IV summarizes the paper.

II. KINEMATIC RESTRICTIONS FOR BACKWARD NUCLEONS

In this section we consider general restrictions on the energy of the backward nucleon emitted at 180° relative to the direction of the projectile proton in $p+A$ reactions in the rest frame of the target nucleus. The restrictions obtained are a consequence of the energy-momentum conservation laws. We are interested in the maximal value of the backward nucleon energy. The production of any additional particles and/or a presence of a nonzero transverse particle momentum in the final state would require extra energy and would cause a reduction of the final energy of the backward nucleon. Thus, to find the maximal value of its energy we assume that no new hadrons are created, and all nucleons move longitudinally. Therefore, our kinematic analysis is reduced to the one-dimensional (longitudinal) problem. Besides, we assume $m=0.94$ GeV for the nucleon mass and neglect the small difference between proton and neutron masses.

A. $R+N\to N+N(180°)$

The energy-momentum conservation in the reaction $p+N\to N+\cdots$ does not permit backward nucleon production in the target nucleon rest frame. If two nuclear nucleons are involved in the $p+A$ reaction the conservation laws for energy and momentum are

$$\sqrt{p^2+m^2}+m+m=\sqrt{k_2^2+m^2}+\sqrt{p_1^2+m^2}+\sqrt{p_2^2+m^2},$$
$$p=p_1+p_2-k_2, \tag{1}$$

where p is the momentum of the projectile proton, $k_2>0$ is the momentum of the backward nucleon $N(180°)$, the lower index in k_2 denotes the number of nuclear nucleons involved, whereas p_1 and p_2 are the final longitudinal momenta of the two nucleons.

Let us denote the maximal value of k_2 as k_2^*. From Eq. (1) and the maxima criteria $\partial k_2/\partial p_1=\partial k_2/\partial p_2=0$, one finds nucleon momenta $p_1=p_2=(p+k_2)/2$ which maximize the backward nucleon momentum $k_2=k_2^*$. This leads to the following algebraic equation for the maximal kinetic energy, $E_2^*\equiv\sqrt{(k_2^*)^2+m^2}-m$, of the backward nucleon:

$$E_2^*=m+\sqrt{p^2+m^2}-2\sqrt{m^2+\left(\frac{p+k_2^*}{2}\right)^2}. \tag{2}$$

The solution of Eq. (2) for the kinetic energy, E_2^*, is presented in Fig. 1(a) by the lower solid (red) line.

The value of E_2^* increases with the projectile proton momentum p, and the upper limit $E_2^*\cong 0.24$ GeV is reached at $p\to\infty$.

We assume that a backward nucleon with kinetic energy E_2^* is created through a two-step process. First, the reaction $p+N\to R+N$ takes place, and a resonance R with the mass M_1 is created. The backward nucleon production then takes place at the second step in the following reaction:[1]

$$R+N\to N(180°)+N. \tag{3}$$

To reach the maximal energy E_2^* [Eq. (2)] of the backward nucleon the baryonic resonance mass M_1 after the first $p+N$ collision should be equal to

$$M_1^2=\left[\sqrt{p^2+m^2}-\sqrt{\left(\frac{p+k_2^*}{2}\right)^2+m^2}+m\right]^2-\left[p-\left(\frac{p+k_2^*}{2}\right)\right]^2. \tag{4}$$

The resonance mass M_1 after the $p+N$ collision is shown in Fig. 1(b) as a function of the projectile momentum p by the lower solid (red) line.

If $n\geqslant 2$ nucleons are involved in the reaction $p+A\to N(180°)+\cdots$ with a backward nucleon production, the energy- and momentum-conservation equations are

$$\sqrt{p^2+m^2}+n\,m=\sqrt{k_n^2+m^2}+\sum_{i=1}^{n}\sqrt{p_i^2+m^2},$$
$$p=\sum_{i=1}^{n}p_i-k_n. \tag{5}$$

Similar to the case of $n=2$, one finds the nucleon momenta $p_1=p_2=\cdots=p_n=(p+k_n)/n$ which maximize the backward nucleon momentum $k_n=k_n^*$. This leads to the following equation for the maximal kinetic energy of the backward nucleon:

$$E_n^*=(n-1)\,m+\sqrt{p^2+m^2}-\sqrt{n^2m^2+(p+k_n^*)^2}. \tag{6}$$

A solution of this equation for $n=3$ is presented in Fig. 1(a) by an upper solid (blue) line. The value of E_3^* increases with the projectile proton momentum p, and the upper limit $E_3^*\cong 0.63$ GeV is reached at $p\to\infty$. Note also that the resulting conservation laws and final expression (6)

[1]Note that the reactions $\Delta+N\to N+N$ were discussed in Ref. [42] where these reactions were proposed as a mechanism of pion suppression in nucleus-nucleus reactions at small collision energies (see also Ref. [43]).

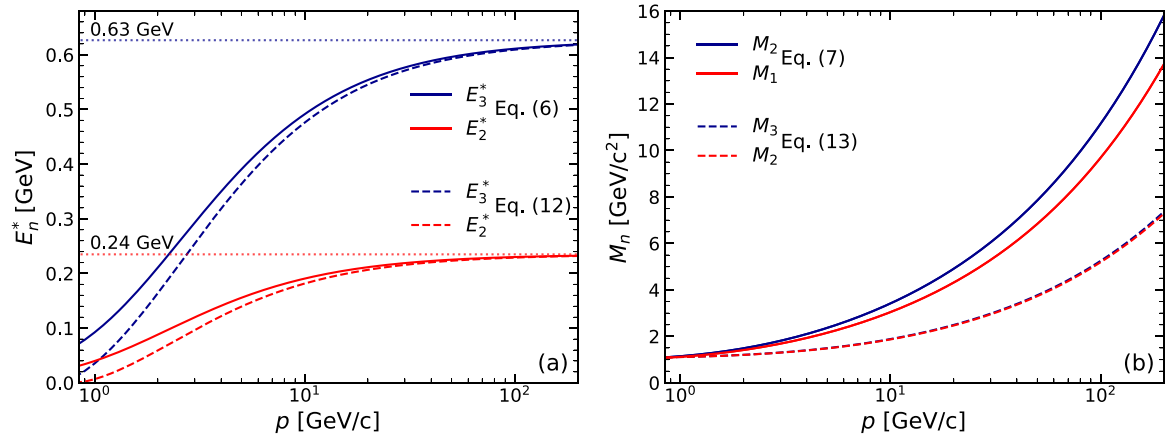

FIG. 1. (a) Maximal kinetic energies E_2^* and E_3^* of the backward nucleons given by Eq. (6) are shown as functions of the projectile proton momentum p by solid red and blue lines, respectively. Horizontal dotted lines show the upper limits at $p \to \infty$. (b) The resonance masses M_1 and M_2 given by Eq. (7) are shown by solid red and blue lines, respectively. Dashed lines on (a) and (b) represent the same quantities but given by Eqs. (12) and (13), when the additional production of a pion, $R \to N(180^\circ) + \pi$, takes place.

for E_n^* are the same as for a collision of the projectile proton with an n-nucleon "grain" in a nucleus.

To produce a backward nucleon with energy E_n^* (6) in reaction (3) a baryonic resonance with mass M_{n-1} needs to be formed in $n-1$ preceding collisions with nuclear nucleons. For example, to reach the energy E_3^* within the reaction (3) the following two preceding reactions have to take place: $p + N \to R_1 + N$ and then $R_1 + N \to R_2 + N$.

The straightforward calculations give

$$M_{n-1}^2 = \left[\sqrt{p^2+m^2} - (n-1)\left(\sqrt{\left(\frac{p+k_n^*}{n}\right)^2 + m^2} - m\right)\right]^2 - \left[p - (n-1)\left(\frac{p+k_n^*}{n}\right)\right]^2. \quad (7)$$

For $n = 2$, Eqs. (6) and (7) are reduced to Eqs. (2) and (4), respectively. The resonance mass M_2 after two successive collisions with nuclear nucleons is shown in Fig. 1(b) as a function of the projectile proton momentum p by the upper solid (blue) line.

From Fig. 1 one observes that E_n^* increases strongly with the projectile proton momentum p up to $p \sim 10$ GeV/c. This corresponds to a mass region of the baryonic resonances not larger than 3–4 GeV. A further strong increase of the baryonic resonance masses at $p > 10$ GeV/c seen in Fig. 1(b) leads to only a slight increase of E_n^* shown in Fig. 1(a).

The momentum of a baryonic resonance with mass M_{n-1} after $n-1$ collisions with nuclear nucleons should be equal to

$$P_{n-1} = p - (n-1)\, p_n = p - (n-1)\,\frac{p+k_n^*}{n}. \quad (8)$$

The solutions of Eq. (8) for $n = 2$ and 3 are presented in Fig. 2 as functions of the projectile proton momentum by the solid upper red and lower blue lines, respectively.

B. $R \to N(180^\circ) + \pi$

Let us assume now a resonance decay into the backward nucleon and pion. If n nuclear nucleons are involved, the conservation laws for the energy and momentum are

$$\sqrt{p^2+m^2} + n\,m = \sqrt{k_n^2+m^2} + \sum_{i=1}^{n}\sqrt{p_i^2+m^2} + \sqrt{p_\pi^2+m_\pi^2}, \quad (9)$$

$$p = \sum_{i=1}^{n} p_i + p_\pi - k_n, \quad (10)$$

where m_π and $p_\pi > 0$ are the pion mass and longitudinal momentum, respectively. At a given value of the projectile

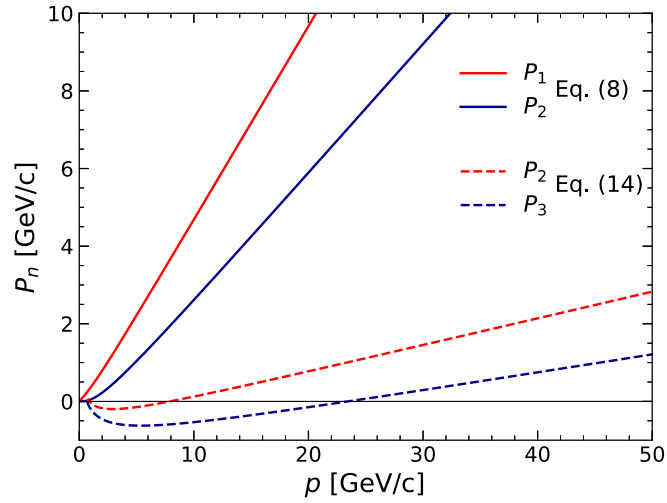

FIG. 2. Solid lines present the momentum P_n [Eq. (8)] of baryonic resonance in reaction $R + N \to N + N(180^\circ)$ for $n = 2$ (upper solid red line) and $n = 3$ (lower solid blue line). Dashed lines present P_n [Eq. (14)] in reaction $R \to N(180^\circ) + \pi$ for $n = 2$ (upper dashed red line) and $n = 3$ (lower dashed blue line).

proton momentum p, the maximal value of the backward nucleon k_n is reached at the conditions $p_1 = p_2 = \cdots = p_n$, and $p_\pi/m_\pi = p_n/m$, i.e., the n nuclear nucleons and created pion should move with the same velocity. The maximal kinetic energy E_n^* of the backward nucleon $N(180^\circ)$ and the mass M_n of a resonance before its decay into the backward nucleon and pion,

$$R \to N(180^\circ) + \pi, \tag{11}$$

are calculated as

$$E_n^* = (n-1)m + \sqrt{p^2+m^2} - \sqrt{(p+k_n^*)^2 + (nm+m_\pi)^2}, \tag{12}$$

$$M_n^2 = \left[\sqrt{p^2+m^2} - n\left(\sqrt{\left(\frac{p+k_n^*}{n+m_\pi/m}\right)^2 + m^2} - m\right)\right]^2 - \left[p - n\left(\frac{p+k_n^*}{n+m_\pi/m}\right)\right]^2. \tag{13}$$

The solutions of Eqs. (12) and (13) for $n = 2$ and $n = 3$ as functions of the projectile proton momentum are presented in Figs. 1(a) and 1(b) by lower (red) and upper (blue) dashed lines, respectively.

The momentum of the baryonic resonance before its decay to the backward nucleons and pions is

$$P_n = p - n\,p_n = p - n\,\frac{p+k_n^*}{n+(m_\pi/m)}. \tag{14}$$

The solutions of Eq. (14) for $n = 2$ and $n = 3$ are presented in Fig. 2 by upper red and lower blue dashed lines, respectively. One can see that the resonance should move backward at small p to produce a backward nucleon with maximal energy.

III. UrQMD SIMULATIONS OF $p + A$ REACTIONS

In this section an analysis of the backward production of protons within the Ultrarelativistic Quantum Molecular Dynamics (UrQMD) transport model [7,8] is performed. The mechanisms of the backward nucleon production by heavy baryonic resonances suggested in previous sections are probed by microscopical simulations of $p + A$ collisions. The UrQMD model performs simulations by the Monte Carlo calculations of stochastic two-particle collisions and resonance decays, and it includes nucleon N^* and Δ resonances with pole masses in the region 1.232–2.250 GeV; higher masses are possible due to the finite widths in Breit-Wigner distribution for unstable particles. The hadron-like states with masses higher than 2.250 GeV are effectively modeled by string excitation; this mechanism is dominant for inelastic hadron collisions at the center-of-mass energy of the nucleon pair $\sqrt{s_{NN}} > 3$ GeV. Contrary to hadronic degrees of freedom, the string degrees of freedom do not interact with other objects; they are only subject to fragmentation.[2] Therefore, in UrQMD simulations the strings are not able to contribute to the suggested mechanism of successive collisions with nuclear nucleons. Within UrQMD the Fermi motion of nucleons is modeled with the random distribution of nuclear nucleon momenta in the range of 0–300 MeV in a nucleus rest frame. The Fermi motion allows widening of the available kinematic region for backward proton production. An another theorized source of cumulative particle production, nuclear short-range correlations [20], cannot be studied within UrQMD because of a lack of implementation of the phenomenon. The implementation of the nuclear short-range correlations in a transport model is still a conceptual problem and a subject for future studies.

For the simulations of $p + A$ energetic collisions the standard setup of UrQMD-3.4 is used. In this setup the mean fields and the hydrodynamic stage of collision are not considered. The backward nucleons are defined as nucleons emitted in a narrow cone with respect to the beam axis, $180^\circ \pm 6^\circ$. The UrQMD simulations are performed in $p + A$ collisions with different nuclei ^{4}He, ^{12}C, and ^{208}Pb at the two values of the projectile proton momenta $p = 6.9$ and $p = 158$ GeV/c. These two momenta correspond to available energies at the Dubna Synchrophasotron and the top energy of the CERN Super Proton Synchrotron, respectively. The backward nucleon production is a rare phenomenon and requires a large sample of events to study energetic cumulative particles. For each $p + A$ reaction a number of $N_{\rm ev} = 10^8$ collision events were simulated. To enlarge a production of the backward nucleons the central $p + A$ collisions with zero impact parameter $b = 0$ are mostly considered. The calculated spectra are presented in Fig. 3. To avoid experimental problems with neutrons, only the backward protons are considered in the analysis. Therefore, a straightforward comparison with experimental data can be done.

The UrQMD results presented in Fig. 3 suggest that the backward proton spectra increase strongly with the atomic number A of the target nucleus. Both the number of backward protons and their largest kinetic energy increase with A. This behavior goes in line with the results from the analysis in Sec. II as the possible number of primary and successive collisions with nuclear nucleons increases strongly with A. The maximal energy of the backward protons does not show a noticeable increase with p from $p = 6.9$ to $p = 158$ GeV/c. This observation just reflects an absence of baryonic resonances with a mass larger than $M > 3$ GeV in the present version of the UrQMD model. An inclusion of resonances with masses larger than $M > 3$ GeV or an implementation of string-hadron interactions in the UrQMD simulations would allow widening of the kinematic range for cumulative particles. This is a point for future studies.

In Fig. 4(a) the UrQMD values of the backward proton spectra at the kinetic energy $E = E_2^* = 0.17$ GeV are presented in $p + A$ collisions at $p = 6.9$ GeV/c as a function of A. Approximating these values by $\approx A^\alpha$ dependence, one finds $\alpha \cong 2.46$ for light nuclei (from He to C) and $\alpha \cong 0.67$ for heavy nuclei (from C to Pb).

The UrQMD results demonstrate also a strong dependence of the backward proton spectra on the centrality in $p + A$ reactions. In Fig. 4(b) we present the backward proton

[2]Note a novel string model for high-energy $p + A$ and $A + A$ collisions where the string-string interactions are considered [44].

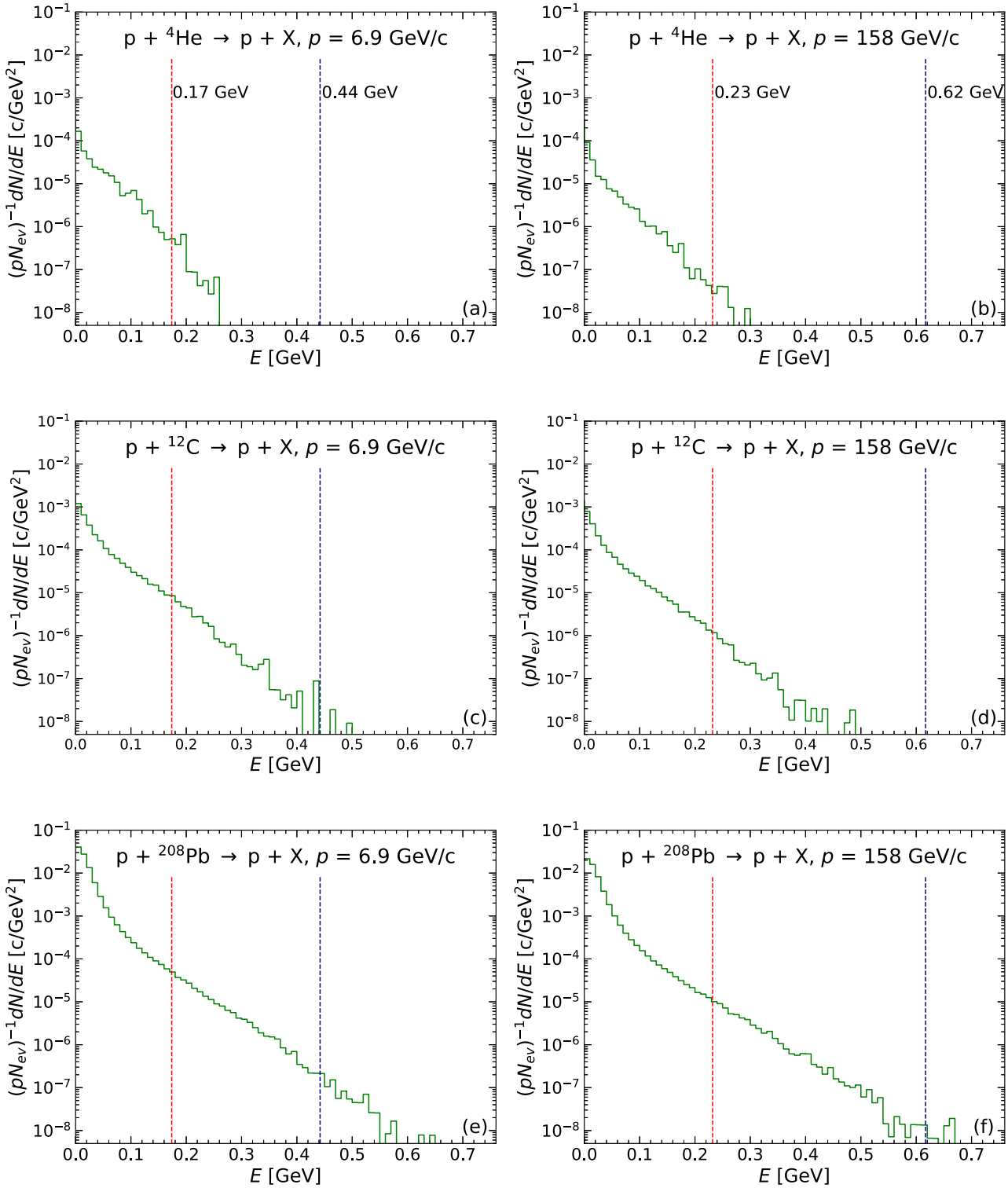

FIG. 3. Spectra of the backward protons as functions of their kinetic energy. For each reaction a sample of $N_{ev} = 10^8$ central collision events with zero impact parameter is used. The vertical dashed lines show the maximum kinetic energies of the backward nucleons at the corresponding initial projectile proton momenta p as calculated with Eq. (6), for collision numbers $n = 2$ (red lines) and $n = 3$ (blue lines).

spectra for UrQMD simulations in p + Cu reactions at the projectile momentum $p = 9.5$ GeV/c. The lower (red) histogram presents the UrQMD results for the peripheral collisions with impact parameter $b = 7$ fm, the upper (yellow) histogram for the central collisions with $b = 0$, while the intermediate (green) histogram for the minimum bias p + Cu reactions. These minimum bias UrQMD results are in a good agreement with the data presented in Ref. [45] and

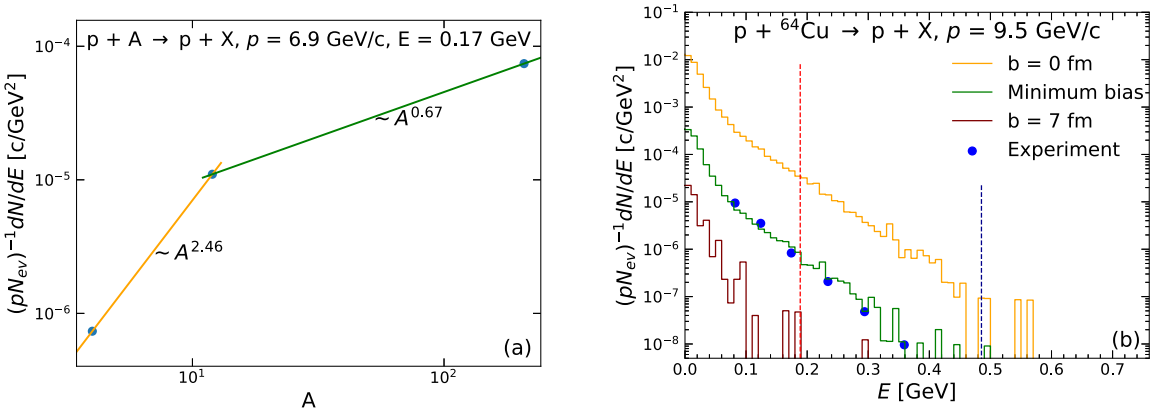

FIG. 4. (a) The backward proton spectra at the fixed kinetic energy $E = E_2^* = 0.17$ GeV in p + He, p + C, and p + Pb collisions at $p = 6.9\,\mathrm{GeV}/c$. (b) Comparison of the UrQMD results for proton spectra at 180° with the data [45] in p + Cu reactions at $p = 9.5\,\mathrm{GeV}/c$. The histograms correspond to the UrQMD results for peripheral ($b = 7$ fm), minimum bias, and central ($b = 0$), from below to up. The vertical dashed lines show the values of $E = E_2^* = 0.19$ GeV and $E = E_3^* = 0.49$ GeV calculated with Eq. (6).

shown in Fig. 4 as full circles. Note, however, that in our calculations a backward proton is defined as observed at angles of $180^\circ \pm 6^\circ$. We have to use an additional normalization factor for the measured data to compare them with our results.

Figures 5(a) and 5(c) show the contributions of different sources to the final spectra of the backward protons as functions of the proton kinetic energy at the projectile proton momentum 158 GeV/c in p + C and p + Pb reactions, respectively. To enlarge the event statistics we define now backward

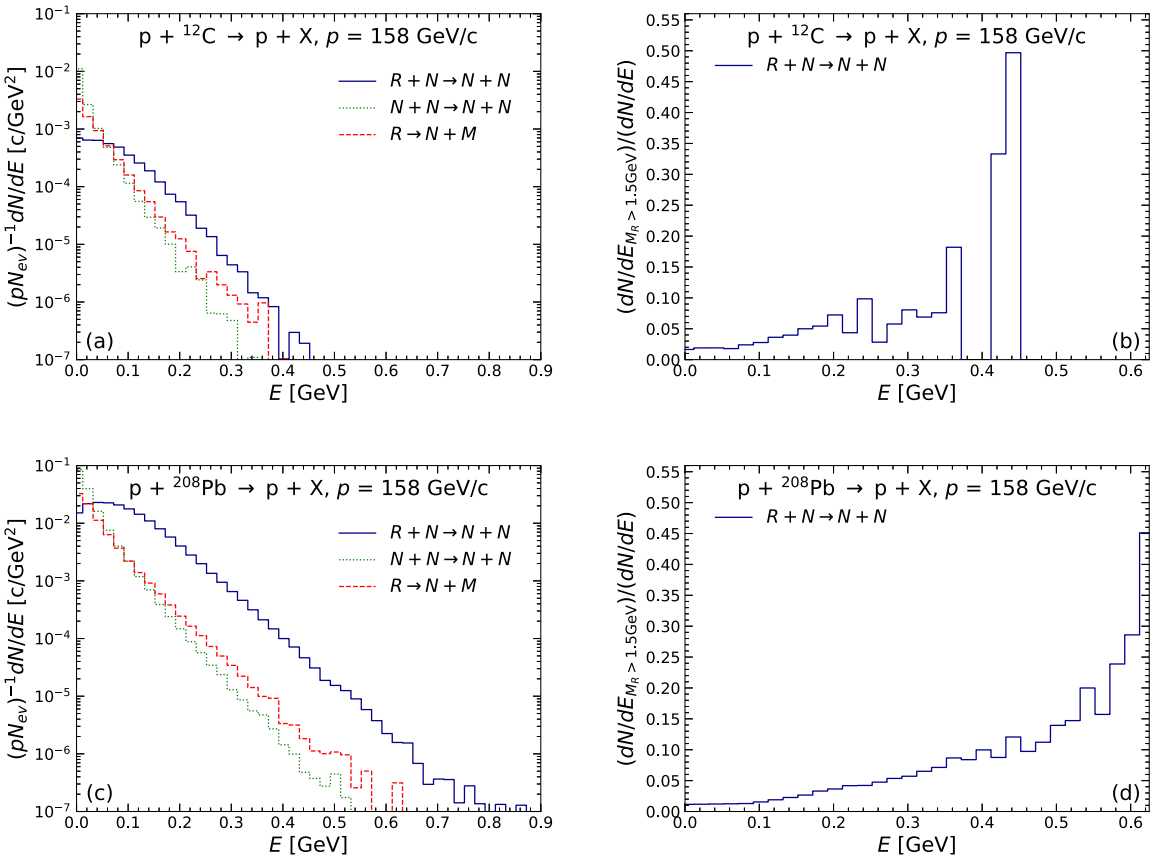

FIG. 5. (a) and (c) The UrQMD spectra of the backward protons ($180^\circ \pm 15^\circ$) produced from the different sources as functions of the backward proton kinetic energy in p + C (a) and p + Pb (c) collisions at the projectile momentum $p = 158\,\mathrm{GeV}/c$. (b) and (d) present the ratios of the spectra of the backward protons created in reactions $R + N \to N + N$ by heavy resonances R with masses $M > 1.5$ GeV to the spectra of all backward protons created in this type of reactions.

protons as being emitted within the cone of backward angles $180^\circ \pm 15^\circ$.

The Fermi motion of nucleons inside nuclei with momenta up to ≈300 MeV is implemented in the UrQMD model. This allows the production of backward nucleons even in a primary $p+N$ collision with the nuclear nucleons. On the other hand, the strong nucleon motion inside the nucleus due to the short-range correlation effects are absent in the present version of the UrQMD model. The multinucleon target grains inside the nucleus are also absent.

From Figs. 5(a) and 5(c) one observes that there are three sources of the backward protons: (multiple) elastic $N+N$ (re)scatterings which take into account the Fermi motion of nuclear nucleons, the resonance decays $R \to N + \cdots$, and the reactions $R+N \to N+N$. At low kinetic energies of the backward proton, elastic (re)scattering effects dominate. On the other hand, at larger E values the backward proton production due to reactions $R+N \to N+N$ becomes the dominant source.

Figures 5(b) and 5(d) show the ratios of the spectra of the backward protons created in reaction $R+N \to N+N$ by resonances with heavy masses $M > 1.5$ GeV to the backward protons produced in this type of reactions by all resonances R with any mass. A partial contribution from heavy resonances with $m > 1.5$ GeV appears to be rather small, but it strongly increases with E.

IV. SUMMARY

The production of backward nucleons $N(180^\circ)$ in $p+A$ collisions in the nuclear target rest frame is studied. This kinematic region is forbidden in $p+N$ reactions. It is suggested that the backward nucleons can be created by heavy baryonic resonances produced in several successive collisions with nuclear nucleons. A baryonic resonance formed in a primary $p+N$ collision propagates through the nucleus and can interact with other nuclear nucleons earlier than it decays. Thus, several nuclear nucleons, $n = 2, 3, \ldots$, are involved in the backward nucleon production. To find the largest possible energy of the backward nucleons in such a scenario the two competitive mechanisms are considered. The first one assumes that the baryonic resonance R is formed in the $n-1$ preceding collisions, and then it creates the backward nucleon in the nth collision via the reaction $R+N \to N(180^\circ)+N$. The second mechanism assumes the baryonic resonance formation in n successive collisions with nuclear nucleons and then its decay into the backward nucleons and pion, $R \to N(180^\circ)+\pi$. In both considered mechanisms, the largest possible energy of the backward nucleon increases with the number of nuclear nucleons involved in the $p+A \to N(180^\circ)+\cdots$ reaction. It also noticeably increases with the projectile proton momentum p up to $p \approx 10\,\mathrm{GeV}/c$ and then goes gradually to its limiting value at $p \to \infty$. The largest energies of the backward nucleon appear to be close to each other in both discussed mechanisms and coincide at $p \to \infty$. However, the masses and longitudinal velocities of baryonic resonances in these two mechanisms are rather different.

Different aspects of backward proton production in $p+A$ reactions are also studied within the UrQMD simulations. The reactions $p+{}^4$He, $p+{}^{12}$C, and $p+{}^{208}$Pb at the projectile momenta $p = 6.9$ and 158 GeV/c, energy at the Dubna Synchrophasotron and the top CERN SPS energy, respectively, are considered. The energy spectrum of the backward protons behaves as $\approx A^\alpha$, where $\alpha \cong 2.46$ for light nuclei and $\alpha \cong 0.67$ for heavy nuclei. We have also found that the maximal energy of the backward proton increases strongly with A.

The UrQMD results show that the decays $R \to N(180^\circ)+\pi$ and the reactions $R+N \to N(180^\circ)$ dominate in the UrQMD production of the backward nucleons with large kinetic energy. The second reaction appears to be the main source of the backward nucleons in p + Pb reactions. This is qualitatively different from the pion backward production considered in Ref. [34] where only resonance decays $R \to \pi(180^\circ)+N$ are permitted.

Short-range p-n correlations inside the nuclei are not implemented in the present version of the UrQMD model. Their implementation would result in a strong increase of particle production in the kinematic regions forbidden in $p+p$ reactions due to the quasielastic collisions of the projectile with nuclear target nucleons. Considered simultaneously, both the short-range correlation effects and inelastic rescatterings of heavy hadron-like states in nuclei are expected to be the competitive mechanisms for a production of final hadrons with momenta forbidden in $p+p$ reactions and for the subthreshold hadron production in low-energy $p+A$ and $A+A$ collisions. We hope that further experimental studies of $p+A$ reactions allow us to search for the new heavy hadron-like states and an extension of the hadron mass spectrum to higher mass values. This research can be done by the NA61/SHINE Collaboration at the SPS CERN as well as in GSI-HADES, and future FAIR-CBM and NICA-MPD experiments. Particularly, the NA61/SHINE Collaboration started the experimental program on the nuclear fragmentation properties. For this purpose, different nuclear projectiles were collided with a proton target at the SPS energies. The test run was successfully done in 2018 [46], and proposals for new measurements in 2021–2024 have been formulated [47]. Within the inverse kinematics of these reactions—high-energy beams of nuclei and a proton target—the backward low-energy proton produced at 180° in the nucleus rest frame becomes the high-energy proton emitted at 0°. This leads to several technical improvements for the detection and precise measurements of these protons. Note also that one of the main goals of the future FAIR-CBM and NICA-MPD experiments is to observe very rare signals in $p+A$ and $A+A$ reactions, e.g., production of multistrange baryons and charmed hadrons at rather moderate collision energies. Thus, they will need to accumulate many millions of collision events. This will be a good chance to observe and study the spectra of protons, pions, and other hadrons outside of the kinematic limits of proton-proton reactions.

ACKNOWLEDGMENTS

The authors are thankful to M. Gazdzicki, M. Strikman, and G.M. Zinovjev for fruitful discussions. The work of M.I.G. is supported by the Goal-Oriented Program of

Cooperation between CERN and National Academy of Science of Ukraine "Nuclear Matter under Extreme Conditions" (Grants Agreement No. CC/1-2019 and No. 0118U005343). H.S. acknowledges support through the Judah M. Eisenberg Laureatus Chair at Goethe University, and the Walter Greiner Gesellschaft, Frankfurt.

[1] R. Hagedorn, Nuovo Cim. Suppl. **3**, 147 (1965).
[2] M. Tanabashi *et al.* (Particle Data Group), Phys. Rev. D **98**, 030001 (2018).
[3] R. Hagedorn and J. Rafelski, Phys. Lett. B **97**, 136 (1980).
[4] M. I. Gorenstein, V. K. Petrov, and G. M. Zinovjev, Phys. Lett. B **106**, 327 (1981).
[5] H. Stoecker, A. A. Ogloblin, and W. Greiner, Z. Phys. A **303**, 259 (1981).
[6] V. Vovchenko, M. I. Gorenstein, C. Greiner, and H. Stoecker, Phys. Rev. C **99**, 045204 (2019).
[7] S. A. Bass *et al.*, Prog. Part. Nucl. Phys. **41**, 255 (1998).
[8] M. Bleicher *et al.*, J. Phys. G **25**, 1859 (1999).
[9] W. Cassing and E. L. Bratkovskaya, Phys. Rev. C **78**, 034919 (2008).
[10] W. Cassing and E. L. Bratkovskaya, Nucl. Phys. A **831**, 215 (2009).
[11] M. Belkacem *et al.*, Phys. Rev. C **58**, 1727 (1998).
[12] B. Andersson, G. Gustafson, G. Ingelman, and T. Sjostrand, Phys. Rep. **97**, 31 (1983).
[13] M. Beitel, K. Gallmeister, and C. Greiner, Phys. Rev. C **90**, 045203 (2014).
[14] A. M. Baldin *et al.*, Yad. Fiz. **18**, 79 (1973).
[15] A. M. Baldin *et al.*, Sov. J. Nucl. Phys. **20**, 629 (1975) [Yad. Fiz. **20**, 1201 (1974)].
[16] R. D. Amado and R. M. Woloshyn, Phys. Rev. Lett. **36**, 1435 (1976).
[17] S. Frankel, Phys. Rev. Lett. **38**, 1338 (1977).
[18] L. L. Frankfurt and M. I. Strikman, Phys. Lett. B **69**, 93 (1977).
[19] L. L. Frankfurt and M. I. Strikman, Phys. Rep. **76**, 215 (1981).
[20] L. L. Frankfurt and M. I. Strikman, Phys. Rep. **160**, 235 (1988).
[21] L. Frankfurt, M. Sargsian, and M. Strikman, Int. J. Mod. Phys. A **23**, 2991 (2008).
[22] A. M. Baldin, Fiz. Elem. Chast. Atom. Yadra **8**, 429 (1977), [296 (1978)].
[23] V. V. Burov, V. K. Lukyanov, and A. I. Titov, Phys. Lett. B **67**, 46 (1977).
[24] A. V. Efremov, Sov. J. Nucl. Phys. **24**, 633 (1976) [Yad. Fiz. **24**, 1208 (1976)].
[25] A. V. Efremov, A. B. Kaidalov, V. T. Kim, G. I. Lykasov, and N. V. Slavin, Sov. J. Nucl. Phys. **47**, 868 (1988) [Yad. Fiz. **47**, 1364 (1988)].
[26] M. A. Braun and V. V. Vechernin, Nucl. Phys. Proc. Suppl. **92**, 156 (2001).
[27] M. I. Gorenstein and G. M. Zinovjev, Phys. Lett. B **67**, 100 (1977).
[28] M. I. Gorenstein, G. M. Zinovjev, and V. P. Shelest, Yad. Fiz. **26**, 788 (1977).
[29] I. G. Bogatskaya, M. I. Gorenstein, and G. M. Zinovjev, Yad. Fiz. **27**, 856 (1978).
[30] I. G. Bogatskaya, C. B. Chiu, M. I. Gorenstein, and G. M. Zinovjev, Phys. Rev. C **22**, 209 (1980).
[31] D. V. Anchishkin, M. I. Gorenstein, and G. M. Zinovjev, Phys. Lett. B **108**, 47 (1982).
[32] E. S. Golubyatnikova, G. A. Shakhanova, and V. L. Shmonin, Acta Phys. Polon. B **15**, 585 (1984).
[33] B. N. Kalinkin and V. L. Shmonin, Phys. Scr. **42**, 393 (1990).
[34] A. Motornenko and M. I. Gorenstein, J. Phys. G **44**, 025105 (2017).
[35] A. Motornenko and M. I. Gorenstein, Acta Phys. Polon. Supp. **10**, 681 (2017).
[36] J. Aichelin and C. M. Ko, Phys. Rev. Lett. **55**, 2661 (1985).
[37] U. Mosel, Ann. Rev. Nucl. Part. Sci. **41**, 29 (1991).
[38] G. Hartnack, L. Sehn, J. Jaenicke, H. Stoecker, and J. Aichelin, Nucl. Phys. A **580**, 643 (1994).
[39] J. Steinheimer and M. Bleicher, J. Phys. G **43**, 015104 (2016).
[40] J. Steinheimer, A. Botvina, and M. Bleicher, Phys. Rev. C **95**, 014911 (2017).
[41] K. Gallmeister, M. Beitel, and C. Greiner, Phys. Rev. C **98**, 024915 (2018).
[42] M. Gazdzicki, M. I. Gorenstein, and S. Mrowczynski, Eur. Phys. J. C **5**, 129 (1998).
[43] H. J. Weyer, Phys. Rep. **195**, 295 (1990).
[44] C. Bierlich, G. Gustafson, L. Lönnblad, and H. Shah, J. High Energy Phys. 10 (2018) 134.
[45] S. Frankel *et al.*, Phys. Rev. C **20**, 2257 (1979).
[46] A. Aduszkiewich *et al.*, (NA61/SHINE Collaboration), CERN-SPSC-2019-041/SPSC-SR-261 (unpublished).
[47] A. Aduszkiewich *et al.*, (NA61/SHINE Collaboration), CERN-SPSC-2018-008/SPSC-P-330-ADD-10 (unpublished).